Determination of AIP/GaP band offset considering conduction-band non-parabolicity of GaP and change in exciton-binding energies ⊘

F. Issiki ✉ (iD) ; Y. Yasutake (iD) ; S. Fukatsu (iD)

Check for updates

View Online

Export Citation

Determination of AlP/GaP band offset considering conduction-band non-parabolicity of GaP and change in exciton-binding energies

View Online　　Export Citation　　CrossMark

F. Issiki,[1,a)] (iD) Y. Yasutake,[2] (iD) and S. Fukatsu[2] (iD)

AFFILIATIONS

[1]Finekit Incorporated, 5-21-17 Kikuna, Kouhoku-ku, Yokohama 222-0011, Japan
[2]Graduate School of Arts and Sciences, The University of Tokyo, 3-8-1 Komaba, Meguro, Tokyo 153-8902, Japan

[a)]Author to whom correspondence should be addressed: f-issiki@finekit.co.jp

ABSTRACT

The well-width (L_z) dependence of photoluminescence (PL) from staggered type-II aluminum phosphide/gallium phosphide (AlP/GaP) indirect-gap quantum wells (QWs) was investigated for determining the AlP/GaP conduction band offset (ΔE_c). The PL spectra at 6 K from a series of type-II QWs with various L_z, 0.06–3.8 nm, grown on GaP(001) substrates showed quantum confinement shifts up to 0.324 eV. The strong conduction-band non-parabolicity reported in GaP was taken into account, and we allowed for a wide range of electron longitudinal effective mass $m_{e\parallel}^*$(GaP) from 0.6 to 4.8 m_0 as a fitting parameter. The exciton-binding energies (E_B) in these QWs were calculated using Leavitte and Little's method [Phys. Rev. B **42**, 11774 (1990)] extended for multiple sub-band mixing, considering the range of the $m_{e\parallel}^*$(GaP). With increasing L_z, the calculated E_B were found to be reduced, and the symmetry of the exciton hole-envelope functions was found to change. The PL peak energies of the wider QWs ($L_z > 1$ nm) agreed with the calculation using $m_{e\parallel}^*$(GaP) = 0.6–1.25 m_0 but did not agree with the calculation using $m_{e\parallel}^*$(GaP) = 4.8 m_0 without considering the non-prabolicity. Correcting the PL peak energies with the calculated E_B, we carefully determined ΔE_c to be 0.374 ± 0.01 eV.

The Al$_x$Ga$_{1-x}$P system is one of a few lattice-matched semiconductor systems [0.3% mismatch between aluminum phosphide (AlP) and gallium phosphide (GaP)] with the indirect bang gap (2.3–2.5 eV) ($0 < x < 1$),[1,2] relatively high refractive indices ($n = 2.8$–3.3),[2] and large optical nonlinearity.[3] GaP has long been used as the base material of green light-emitting diodes.[4] The conduction-band minima in both AlP and GaP are near the X points in the momentum space, while the valence-band top is at the Γ point. The AlP/GaP interface forms a staggered type-II band structure where electrons and holes are separated at the interface.[5] When a quantum well (QW) is created with layers of different compositions x in the Al$_x$Ga$_{1-x}$P system, it becomes a type-II QW. The optical transition in such a structure is then double-forbidden in the real and momentum spaces. However, it has been clarified that by devising quantum confined structures, it is possible to induce quantum effects such as Γ–X mixing[6] and significantly increase optical activity selectively in a targeted layer, enabling fabrication of light emitters and/or photodetectors within a monolithic structure. In fact, quite low optical-absorption loss in transparent GaP and AlGaP crystals enables the fabrication of complex optical devices with thick films grown by epitaxy, taking advantage of the lattice-matched system. The AlGaP system has been gaining attention for its ability to create monolithically formed integrated optical devices such as optical resonators,[7] frequency comb generators with second-harmonic conversion,[8,9] and light-emitting devices with distributed Bragg reflectors.[10] The AlGaP system is also expected to provide basic research insights into how indirect semiconductors such as silicon and silicon germanium can be applied to optical devices.[11–13]

Accurate band offsets are important for the correct wavelength-response design of these devices and are necessary for optical and electrical evaluations in basic research. Designing and fabricating devices with precisely targeted band offsets can improve wavelength selectivity, yield, and reliability.

Our reexamination of the AlP/GaP conduction band offsets (ΔE_c) has been motivated by the large mismatch of >100 meV in the photoluminescence (PL) peak energies of an AlGaP structure found between the experiment and calculation in 1995.[6] Three possible issues had been assumed as the causes of the large mismatch; the first issue was the experimentally unknown AlP electron effective mass at that

01 July 2025 20:30:36

time, and the best-fit value in our experiment was much different from the theoretical values, as Vurgaftman and Meyer pointed out.[1] This issue was addressed in 2008 by Semtsiv et al.,[14] who determined $m_{e\parallel}^*(\text{AlP}) = 0.90\,m_0$ and $m_{e\perp}^*(\text{AlP}) = 0.30\,m_0$ over the hurdles of the AlP deliquescence,[15] where the $m_{e\parallel}^*$ is the effective mass of electrons in the longitudinal direction <001>, and $m_{e\perp}^*$ is the effective mass in the transverse (lateral) directions <100> and <010>, and m_0 is the free electron mass. It should also be noted that even the exciton-binding energy (E_B) in bulk AlP has not yet been established.

The second issue was the possible mismatch of the ΔE_c, as we had used ΔE_c measured at room temperature (RT)[5] in the comparison with the PL results at 6 K in 1995. Later, Nagao et al. reported $\Delta E_c = 0.38$ eV at 4 K in 1997 assuming fitting parameter $m_e^*(\text{AlP}) = 0.85\,m_0$.[16] Their ΔE_c was assumed to be a much better value, although the changes in the E_B were not explicitly considered in their evaluation. The E_B in bulk GaP had been reported to amount to as much as 0.0215 eV (Refs. 2 and 17) and would be reduced in staggered type-II QWs, then it would be more favored that the amount of the change be taken into account in the evaluation by Nagao et al. Even after their report, calculated ΔE_c values were also cited and differed.[18,19] It seems, then, that there is still demand for further reliable ΔE_c values.

The third issue was the strong non-parabolicity of GaP conduction-band bottoms,[20] which might lead to large changes in $m_e^*(\text{GaP})$ and affect the confinement energies of electrons in the AlP/GaP QWs as well as the $m_{e\parallel}^*(\text{AlP})$. Miura et al. reported $m_{e\parallel}^*(\text{GaP})$ varying from 4.8 to 6.9 m_0 with the change in measuring condition, while $m_{e\perp}^*(\text{GaP})$ was found to be stable at around 0.25 m_0.[20] The large values and changes in $m_{e\parallel}^*(\text{GaP})$ were explained to be due to the so-called camel's back structure, i.e., the W-shaped two-hump conduction-band bottoms split across the X points caused by the lack of inversion symmetry in the GaP crystal.[20] In AlP QWs, the actual GaP barrier effective mass $m_{e\parallel}^*(\text{GaP})$ of the confined states would change from the band-bottom values, because the energy levels of the confined states in the QWs would be lower than those barrier GaP-band bottoms by more than 0.2 eV in wider wells, and the effects of the two-hump band bottoms would decrease. Park and Chang calculated $m_{e\parallel}^*(\text{AlP})$ to be 0.92 m_0 and $m_{e\parallel}^*(\text{GaP})$ to be 1.25 m_0 in their AlP/GaP superlattice models,[21] showing the possibility of a much-reduced $m_{e\parallel}^*(\text{GaP})$. In our determination, therefore, we assumed that the $m_{e\parallel}^*(\text{GaP})$ would be better treated as a fitting parameter, allowing for a wide enough range of $m_{e\parallel}^*(\text{GaP})$. The non-parabolicity was found to affect the well-width (L_z) dependence of the QWs in our calculation, which we discuss later in this Letter.

In this Letter, we revisit these issues and report our ΔE_c determination considering the non-parabolicity of the GaP conduction band and change in the E_B. We first present the PL results from several AlP/GaP QWs of various widths. We then calculate the E_B in those QWs for correcting the excitonic effects in the PL. We graphically estimate the AlP-conduction-band bottom energy from a PL-peak-shift analysis. We allow for a wide range of $m_{e\parallel}^*(\text{GaP})$, 0.6–4.8 m_0, and consider the minimum and maximum $m_{e\parallel}^*(\text{GaP})$ in both the E_B calculation and the PL-peak-shift analysis of actual QWs. We also allow for a change in $m_{e\parallel}^*(\text{AlP})$ in the PL-peak-shift analysis, as it was considered to sensitively affect the ΔE_c-determination. Finally, we determine the ΔE_c and recheck the consistency of those ranges.

The samples were AlP/GaP multiple QWs (MQWs) grown by gas source molecular beam epitaxy (VG Semicon V80H) using PH$_3$

and elemental Ga and Al. The substrates were nominally undoped GaP (001). The structure of a typical sample is illustrated in the inset of Fig. 1. After the growth of a 200-nm GaP buffer layer, a 10-period AlP(20 nm)/GaP(20 nm) multilayer and AlP/GaP MQWs with various L_z were grown. A satellite peak analysis of the x-ray diffraction from the multilayers was used to calibrate the layer thicknesses. The L_z were inferred from the exposure time. The GaP barrier was 50 nm thick. The growth temperature was 620 °C, which was the lowest temperature at which clear 4× patterns in the reflection high energy electron diffraction (RHEED) can be observed through the growth of the whole structure. The RHEED 4× pattern was a signature of good crystalline quality and flat interface morphology.[22] No growth interruption was performed at the interfaces. Post-growth annealing was conducted at 650 °C for 3 min to ensure the layers were of high quality. PL was measured at 6 K by using a 405-nm continuous-wave indium-aluminum-gallium-nitride laser. The optical power density was carefully selected between 0.03 and 0.1 W/cm^2 to avoid peak broadening.[23] We had separately confirmed stable single-peak excitonic luminescence from each QW without the peak broadening at the power densities between 0.01 and 0.8 W/cm^2.

Figure 1 compares the PL spectra from the AlP/GaP MQW samples. Well-resolved peaks were captured from the QWs with $L_z = 0.06$–3.8 nm. The QWs of $L_z = 0.06$ and 0.13 nm are sub-monolayer (ML) QWs. The main peak from each QW can be assigned to the no-phonon (NP) line.[24] Its phonon replicas due to both longitudinal optical and transverse optical phonons[24] can be found on the lower energy side in the spectra of 0.06-, 0.13-, 0.27-, and 0.69-nm QWs. The systematic peak shifts of the sub-ML QWs indicate large excitonic radii in the lateral directions, spread over several Al and Ga atoms and reflecting their averaged potential. The quantum-confinement shift amounted to 0.324 eV, from 3.8 nm (1.984 eV) to 0.06 nm (2.308 eV) in L_z, which was already well over the reported ΔE_c at RT.[5,25] The bulk GaP band edge is visible at 2.319 eV in the spectra of 1.2–2.7-nm MQWs and at the foot of the 0.13-nm QW peak. Such an NP transition in bulk often occurs with shallow impurities; thus, the decrease in the emission energy that was 9 meV below the known excitonic bandgap of GaP, 2.328 eV,[17] would naturally be counted as the possible trapping energies of the shallow impurities.

FIG. 1. 6-K PL spectra of AlP/GaP MQWs with well widths (L_z) of 0.06–3.8 nm. Inset shows the structure of a typical sample. Small features observed on lower energy side of prominent no-phonon peak are its phonon replicas. Peaks higher in energy than those of 0.27-nm QW are attributed to sub-monolayer (ML) QWs. Systematic peak shifts are observed.

This 9-meV discrepancy is mentioned later in this Letter. The faint luminescence peak from the bulk AlP whose peak is at 2.489 eV can also be assigned to the shallow-impurity peak from the multilayer AlP.

We then calculate the E_B for correcting the PL results.

Figure 2 shows the calculated E_B plotted against L_z. Figure 3 schematically shows the envelope functions of the electron and hole. In the calculation of E_B, we used a one-dimensional single-band envelope function approach and the method developed by Leavitte and Little[26] and extended it for counting the mixing of 50 sub-bands each for electrons and holes, as detailed in the supplementary material. In Figs. 2 and 3, the solid and dashed lines are the upper and lower bounds to E_B, which are largely controlled by the relative permittivity (dielectric constant) ϵ_r and $m^*_{e\parallel}$, where the ϵ_r values are in units of the vacuum permittivity. We considered the $m^*_{e\parallel}(GaP)$ of 0.6–4.8 m_0, possible range of the other m^*_e and m^*_h in the bulk and QWs, and mixing of both the static (ϵ_0) and dynamic (ϵ_∞) permittivities in the excitonic states as described in a classical picture of Haken.[27] For the upper bound, $m^*_{e\parallel}(GaP) = 4.8\, m_0$,[20] $m^*_{hh\parallel}(GaP) = 0.325\, m_0$,[1] $\epsilon_r(GaP) = \epsilon_\infty(GaP) = 8.9$,[2] $m^*_{hh\parallel}(AlP) = 0.52\, m_0$,[1] and $\epsilon_r(AlP) = \epsilon_\infty(AlP) = 7.54$[2] were used. For the lower bound, $m^*_{e\parallel}(GaP) = 0.6\, m_0$, $m^*_{hh\parallel}(GaP) = 0.22\, m_0$,[1] $\epsilon_r(GaP) = \epsilon_0(GaP) = 10.86$,[28] $m^*_{hh\parallel}(AlP) = 0.25\, m_0$,[1] and $\epsilon_r(AlP) = \epsilon_0(AlP) = 9.84$[2] were used. Note that $m^*_{e\perp}(GaP) = 0.253\, m_0$,[20] $m^*_{hh\perp}(GaP) = 0.325\, m_0$,[1] $m^*_{e\parallel}(AlP) = 0.90\, m_0$,[14] $m^*_{e\perp}(AlP) = 0.30\, m_0$,[14] and $m^*_{hh\perp}(AlP) = 0.52\, m_0$[1] were commonly used for both. The valence band offset (ΔE_v) was obtained through the relation $\Delta E_v = \Delta E_c + E_g(AlP) - E_g(GaP)$ by using $E_g(AlP) = 2.505$ eV (Ref. 29) and the ΔE_c to be determined later.

As shown in Fig. 2, the E_B for AlP/GaP type-II QWs monotonically decreased with increasing L_z. Note that this is in contrast with typical type-I QWs, where E_B often goes through a maximum at intermediate well widths, reflecting the increased binding energies of two-dimensional excitons. The actual $E_B = 21.5$ meV for the bulk GaP,[17] is found in the middle between the upper and lower bounds at $L_z = 0$, which is consistent with the picture of Haken.[27] The calculated E_B, 6.2–10.4 meV, for QW with $L_z = 3.8$ nm appear comparatively small as expected.

In Fig. 3, the envelope functions in (a) GaP bulk ($L_z = 0$), AlP/GaP QWs with (b) $L_z = 0.06$, (c) $L_z = 1.2$, (d) $L_z = 3.8$ nm, and (e) a type-II AlP/GaP single heterostructure are shown. For small L_z, the envelope functions were symmetric. The symmetry, however, started to change between 1.2 and 1.5 nm, as electrons or holes began to accumulate on either side of the QW in favor of an increased E_B. This would be intuitively clear in view of the staggered type-II single interface (e) as the limiting case of $L_z = \infty$. The wave functions of the lower bound of E_B (dotted lines) were more spread out in the growth direction (z-axis) than those of the upper bound of E_B (solid lines), which is also consistent with the classical picture of the excitonic states.

We then plot these results (the calculated E_B) with the PL peak energies in Fig. 4.

Figure 4(a) shows the energies of the main PL peaks vs L_z, while Fig. 4(b) is a replot as a function of L_z^{-2}. Such a rescaling helps reveal a slope proportional to the inverse effective mass m_e^{*-1}, provided that the barrier penetration of wave functions is negligibly small at larger L_z values. The solid circles show the energies of the main PL peaks in Fig. 1. The open circles are shifted upward from the solid ones by the calculated E_B of the upper and lower bounds. As shown in Fig. 4(b), the solid and open circles eventually fall on the lines with increasing L_z. Extrapolating the solid circles for the 1.8-, 2.7-, and 3.8-nm QWs to the vertical axis, we can estimate the PL peak energy $E = 1.968$ eV from the intercept in the limit $L_z = \infty$. If a constant E_B is assumed,

FIG. 2. L_z dependence of the calculated exciton-binding energy (E_B). Upper bound (solid line) and lower bound (dashed line) are shown. Actual GaP bulk E_B is in the middle between upper and lower bounds of calculation at $L_z = 0$. Note that type-II AlP/GaP QWs show steady decrease in E_B with increasing L_z.
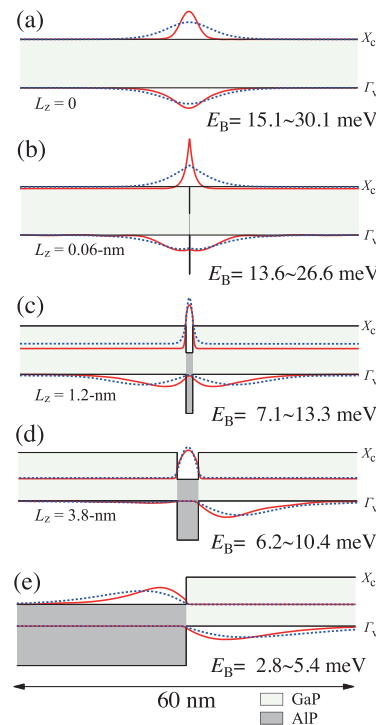

FIG. 3. Envelope functions of electron and hole in exciton in (a) bulk GaP, (b) 0.06-nm QW, (c) 1.2-nm QW, (d) 3.8-nm QW, and (e) AlP/GaP single heterostructure. Solid and dashed lines correspond to upper and lower bounds of E_B, respectively. Symmetry of hole envelope function changes with increasing L_z.
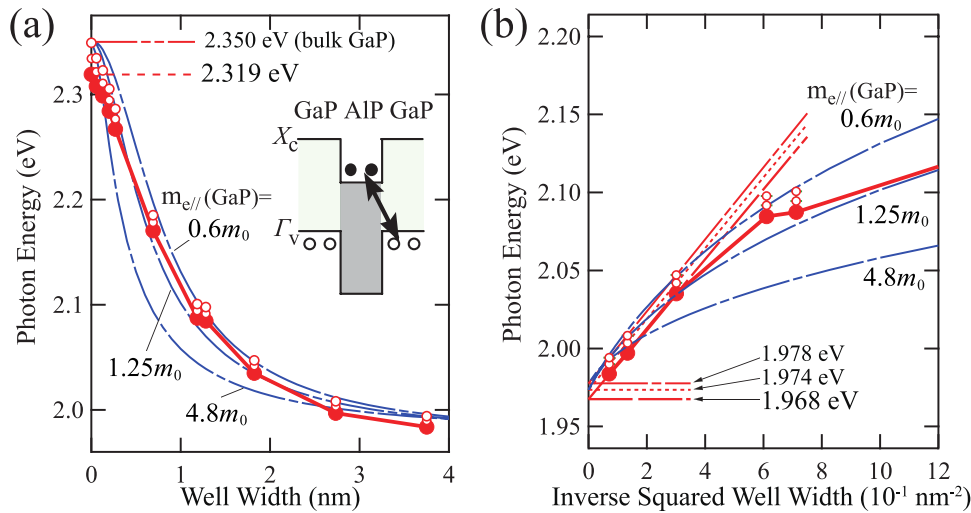
FIG. 4. Energies of main PL peaks as functions of (a) L_z and (b) L_z^{-2}. Solid circles show as-recorded PL peak energies, while open circles show those with corrections due to E_B. Inset shows schematic potential profile of AlP/GaP type-II QWs. The solid and open circles in (b) eventually fall on lines with increasing L_z. Extrapolation of data for 1.8-, 2.7-, and 3.8-nm QWs to vertical axis provides transition energies of 1.968 eV (*uncorrected*), 1.974 eV (corrected with smallest E_B estimate), and 1.978 eV (corrected with largest E_B estimate) for the limiting case $L_z = \infty$. Curved lines for $m_{e\parallel}^*$(GaP) $= 4.8\,m_0$ clearly fall short of PL peak energies in (b), indicating non-parabolicity of $m_{e\parallel}^*$(GaP).

ΔE_c can roughly be estimated to be 0.360 (=2.328–1.968) eV at this stage.

Similarly, by extrapolating the open circles to the vertical axis, we can find 1.978 eV for the upper bound and 1.974 eV for the lower bound of E_B. These values are the energy levels of the estimated AlP-conduction-band bottom and energy gaps from the GaP-valence-band top. Subtracting these from the reported optical (non-excitonic) bandgap, E_g(GaP) = 2.350 eV,[17] one finds 0.372 (=2.350 − 1.978) eV for the upper bound and 0.376 (=2.350 − 1.974) eV for the lower bound. We, thus, have ensured the AlP/GaP band offset to be $\Delta E_c = 0.374 \pm 0.01$ eV. The 0.01 eV uncertainty allows for not only the difference between the spread of E_B values (± 0.002 eV) but also the possible trapping potential of the shallow impurities of ≤ 9 meV to be recounted.

Finally, we rechecked the ranges of $m_{e\parallel}^*$(GaP) and $m_{e\parallel}^*$(AlP) assumed in Figs. 2 and 3. We calculated the L_z dependence with the obtained ΔE_c within the effective mass approximation assuming the square potential for AlP/GaP QWs. The effect of interface blurring in the QWs was calculated to be negligible and is also explained in the supplementary material. We assumed ideally square potential in the calculation, as the final errors in the determined ΔE_c due to the effect of interface blurring would be as small as 0.2 meV and negligible, even if we assumed 1-ML blurring of Al and Ga atoms at every AlP/GaP interface. The estimate of this effect is also explained in the supplementary material. The results are plotted in Figs. 4(a) and 4(b) with the dashed-solid curved lines for three $m_{e\parallel}^*$(GaP) values, 0.6, 1.25, and 4.8 m_0 with fixed $m_{e\parallel}^*$(AlP) = 0.90 m_0. The curved lines in Fig. 4(b) provide a reasonable fit with $m_{e\parallel}^*$(GaP) = 0.6–1.25 m_0, which is within the range covered by the upper and lower bounds. The results are also in good agreement with $m_{e\parallel}^*$(GaP) = 1.25 m_0 predicted by Park and Chang.[21] The curved lines drawn using $m_{e\parallel}^*$(GaP) = 4.8 m_0 in Fig. 4(b) clearly fall short of the PL peak energies and fail to reproduce the L_z dependence of the wider AlP QWs ($L_z > 1$ nm). This indicates that the $m_{e\parallel}^*$(GaP) was changed in the QWs of wider L_z due to the non-parabolicity. The effective mass $m_l = 0.91\,m_0$ before the band splitting of X_1 and X_3 estimated by Miura *et al.*[20] was within the range of $m_{e\parallel}^*$(GaP) = 0.6–1.25 m_0.

We should also note that the slopes of the fitting lines in Fig. 4(b) could also be reproduced using $m_{e\parallel}^*$(AlP) $\approx 1.5\,m_0$ in the absence of the barrier penetration, i.e., if we assumed the infinite barrier height on both sides of the QWs. The apparent slope was affected by the barrier effective mass.

As pointed out by Park and Chang[21] and by Semtsiv *et al.*,[14] an AlP film grown on a GaP (001) substrate is compressively strained in the lateral directions, and the indirect valleys X_x, X_y, and X_z split into the longitudinal X_z and the twofold transverse valleys, X_x and X_y. The X_z valley has a heavy mass in the z direction $m_{e\parallel}^*$, while the X_x and X_y valleys have a light mass in the z direction $m_{e\perp}^*$, then the X_z bound states are formed in the QWs of $L_z < 4$ nm, compensating for the strain-induced upward shift of the X_z band edge. The uniaxial pressure dependence of PL from AlP/GaP superlattice structures[30] is consistent with this view. Thus, we infer that the obtained ΔE_c was the offset between the X_z valleys in the AlP layers and X valleys in the unstrained GaP layers. The bulk AlP peak in Fig. 1 can naturally be assigned to X_x and X_y valleys in the same manner.

In conclusion, we have investigated the L_z dependence of PL of AlP/GaP type-II QWs grown on GaP (001) substrates. The PL showed maximum quantum confinement shift of 0.324 eV. The E_B in the QWs were calculated using Leavitte and Little's method extended for sub-band mixing treatment, and found to be reduced in the wider QWs. The PL results agreed with the calculation with the smaller $m_{e\parallel}^*$(GaP), indicating the non-parabolicity of the GaP conduction band. By extrapolating the data for the wider L_z corrected by the calculated E_B, we determined the conduction band offset of the AlP/GaP interface to be $\Delta E_c = 0.374 \pm 0.01$ eV at 6 K.

See the supplementary material for details of the E_B calculation method and estimated effect of interface blurring.

AUTHOR DECLARATIONS

Conflict of Interest

The authors have no conflicts to disclose.

Author Contributions

F. Issiki: Data curation (lead); Formal analysis (lead); Funding acquisition (supporting); Investigation (lead); Methodology (lead); Visualization (lead); Writing – original draft (lead). **Y. Yasutake:** Data curation (supporting); Resources (supporting); Supervision (supporting); Writing – review & editing (equal). **S. Fukatsu:** Funding acquisition (lead); Resources (lead); Supervision (lead); Writing – review & editing (equal).

DATA AVAILABILITY

The data that support the findings of this study are available within the article.

REFERENCES

[1] I. Vurgaftman, J. R. Meyer, and L. R. Ram-Mohan, J. Appl. Phys. **89**, 5815 (2001).

[2] *Landort-Börnstein: Numerical Data and Functional Relationships in Science and Technology*, edited by O. Madelung (Springer, Berlin, 1987).

[3] I. Shoji, T. Kondo, and R. Ito, Opt. Quantum Electron. **34**, 797 (2002).

[4] J. Nishizawa, Y. Okuno, M. Koike, and F. Sakurai, Jpn. J. Appl. Phys., Part 1 **19**, 377 (1980).

[5] J. R. Waldrop, R. W. Grant, and E. A. Kraut, J. Vac. Sci. Technol., B **11**, 1617 (1993).

[6] F. Issiki, S. Fukatsu, and Y. Shiraki, Appl. Phys. Lett. **67**, 1048 (1995); **68**, 431 (1996).

[7] M. Billet, L. Reis, Y. Léger, C. Cornet, F. Raineri, I. Sagnes, K. Pantzas, G. Beaudoin, G. Roelkens, F. Leo, and B. Kuyken, Opt. Mater. Express **12**, 3731 (2022).

[8] A. D. Logan, M. Gould, E. R. Schmidgall, K. Hestroffer, Z. Lin, W. Jin, A. Majumdar, F. Hatami, A. W. Rodriguez, and K.-M. C. Fu, Opt. Express **26**, 33687 (2018).

[9] D. J. Wilson, K. Schneider, S. Hönl, M. Anderson, Y. Baumgartner, L. Czornomaz, L. T. J. Kippenberg, and P. Seidler, Nat. Photonics **14**, 57 (2020).

[10] K. Hestroffer, D. Sperlich, S. Dadgostara, C. Golz, J. Krumland, W. T. Masselink, and F. Hatami, Appl. Phys. Lett. **112**, 192107 (2018).

[11] M. J. Chen, J. L. Yen, J. Y. Li, J. F. Chang, S. C. Tsai, and C. S. Tsai, Appl. Phys. Lett. **84**, 2163 (2004).

[12] S. G. Cloutier, P. A. Kossyrev, and J. Xu, Nat. Mater. **4**, 887 (2005).

[13] N. Usami, F. Issiki, D. K. Nayak, and Y. Shiraki, Appl. Phys. Lett. **67**, 524 (1995).

[14] M. P. Semtsiv, O. Bierwagen, W. T. Masselink, M. Goiran, J. Galibert, and J. Léotin, Phys. Rev. B **77**, 165327 (2008).

[15] H. G. Grimmeiss, W. Kischio, and H. Scholz, Philips Tech. Rev. **26**, 136 (1965).

[16] S. Nagao, T. Fujimori, H. Gotoh, H. Fukushima, T. Takano, H. Ito, S. Koshihara, and F. Minami, J. Appl. Phys. **81**, 1417 (1997).

[17] R. G. Humphreys, U. Rössler, and M. Cardona, Phys. Rev. B **18**, 5590 (1978).

[18] N. N. Ledentsov, V. A. Shchukin, J. Lyytikäinen, O. Okhotnikov, Y. M. Shernyakov, A. S. Payusov, N. Yu. Gordeev, M. V. Maximov, S. Schlichting, F. Nippert, and A. Hoffmann, Appl. Phys. Lett. **105**, 181902 (2014).

[19] O. P. S. Filho, M. Ribeiro, Jr., R. R. Pelá, L. K. Teles, L. G. Ferreira, and M. Marques, J. Appl. Phys. **114**, 033709 (2013).

[20] N. Miura, G. Kido, M. Suekane, and S. Chikazumi, J. Phys. Soc. Jpn. **52**, 2838 (1983).

[21] C. H. Park and K. J. Chang, Phys. Rev. B **47**, 12709 (1993).

[22] *Characterization of Materials*, edited by E. N. Kaufmann (John Wiley and Sons, Hoboken, NJ, 2012), p. 1928.

[23] S. Bhuyan, R. Mondal, P. Khatua, M. Semtsiv, W. T. Masselink, J. Léotin, B. Pal, and B. Bansal, J. Appl. Phys. **114**, 163101 (2013).

[24] F. Issiki, S. Fukatsu, T. Ohta, and Y. Shiraki, Solid-State Electron. **40**, 43 (1996).

[25] A. Morii, H. Okagawa, K. Hara, J. Yoshino, and H. Kukimoto, Jpn. J. Appl. Phys., Part 2 **31**, L1161 (1992).

[26] R. P. Leavitt and J. W. Little, Phys. Rev. B **42**, 11774 (1990).

[27] R. S. Knox, "Theory of excitons," in *Solid State Physics, Supplement 5* (Academic Press, New York, 1963).

[28] G. A. Samara, Phys. Rev. B **27**, 3494 (1983).

[29] B. Monemar, Phys. Rev. B **8**, 5711 (1973).

[30] K. Uchida, N. Miura, J. Kitamura, and H. Kukimoto, Phys. Rev. B **53**, 4809 (1996).